

Electronic properties of fractal-glass models

William A. Schwalm and Mizuho K. Schwalm

Department of Physics, University of North Dakota, Grand Forks, North Dakota 58202

(Received 23 January 1989)

Analytic results are presented for four new fractal lattices. A basic similarity between fractals and homogeneous glassy networks is the fluctuating environments of the lattice sites. The fractals are classified in terms of their local bonding geometry by comparison with glassy networks: (1) amorphous graphite, (2) two-dimensional and (3) three-dimensional Zachariasen glasses of two components, and (4) a three-component, infinitely ramified glass model with fractal dimension $\bar{d} \approx 3$ and spectral dimension $\bar{d} > 2.5$. Localization and size scaling of corner-to-corner propagation are investigated, and it is found that there is a transition from power-law to exponential dependence in the case of model (1) at a correlation length $\lambda \approx 64$. Edge states appear to play an important role in propagation over distances longer than λ . Effects of ring closure and site variety are studied by making two modifications to model (1). In the first, branch cuts unroll the ring structure into a Bethe lattice. In the second, the rings are severed, resulting in a fractal tree. Results suggest that noncontinuum spectral structure is more closely related to site variety than to connectedness or ring closure in these fractal-glass models. This is similar to Anderson localization in the homogeneous random case.

I. INTRODUCTION

Analytic solutions for Green functions of several new fractal lattices are presented here. The results are used to study properties of amorphous structures that are glass-like and hierarchical.

Amorphous materials having short-range order due to bonding constraints but lacking long-range order are generally sorted into three categories.¹⁻⁴ These are (1) *substitutional disorder*, in which atoms are substituted randomly on a lattice with translation symmetry, (2) *positional disorder*, in which atomic positions are randomly distributed, and (3) *topological disorder*. The latter is a particular kind of positional disorder distinguished in the case of amorphous semiconductors because of the special role played by the bonding network in determining the properties of these substances.¹ A tight-binding model Hamiltonian for an amorphous semiconductor is a mathematical model determining one-electron properties, and at the same time its nonvanishing matrix elements define a neighborhood structure. Two sites are neighbors if H has an element connecting them. Thus, H expresses a relationship between topology of the lattice and properties of the model.

Each of the three classifications listed above tacitly presumes a kind of homogeneity that the network models treated below do not have. The density of atoms is constant, for example, and though the neighborhoods of the sites fluctuate, the distribution of neighborhoods is assumed not to be a function of position.⁵ Each of these classes of disorder can thus be called homogeneous.

In contrast, it has been proposed that certain amorphous structures including granular semiconductors and diffusion aggregates are better modeled by scaling fractal networks.^{6,7} These are not homogeneous but are perforated by voids on every length scale in such a way that

the density is not constant. The number of sites N depends on the network diameter L according to $N \sim L^{\bar{d}}$, where \bar{d} is the fractal dimension.⁶ The models treated below are of this kind.

In the work reported here we assume there are granular semiconductors or amorphous carbon networks such as soot or charcoal which, because they have a scaling pore structure consisting of a distribution of voids of all sizes, are trema fractals down to the atomic length scale.⁶ Small-angle x-ray-scattering data from lignite coal have been interpreted as due to fractal pore structure.⁸ The fractal nature of lignite may have to do with the surface rather than the volume of the pores, and it is clear that density is not a function of size in macroscopic samples. It is nevertheless interesting to explore the properties of scaling fractal models with local bonding geometry like that of graphite or of semiconductor materials in order to see how they are similar to or different from the homogeneous cases.

The inhomogeneous models called fractal glasses below have two essential properties. They are trema fractals with a scaling distribution of pore sizes. Also, as in the case of a random network, there is great variety in the site environments. Figure 1(a) shows part of a random fractal-glass model for amorphous graphite. The hierarchical model of Fig. 1(b), though not random, has in common with the random case the two important properties of a scaling-void distribution and site variety. To support this claim, a digression site variety is in order.

In crystals with translation symmetry there are unit cells in which a given site has the same environment or set of neighborhoods as the corresponding site in any other cell. In both Figs. 1(a) and 1(b), neighborhoods are varied. In fact, when arbitrarily large neighborhoods are considered, the sites of Fig. 1(b) are unique modulo the overall C_{3v} symmetry of the lattice.

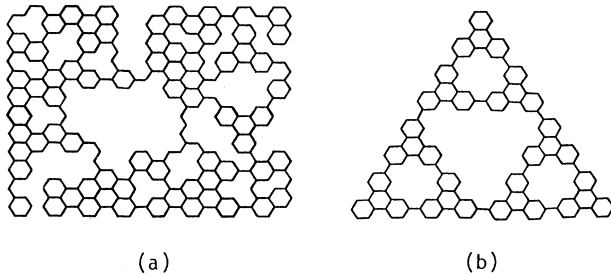


FIG. 1. (a) Amorphous and (b) ordered fractal-glass models for graphite.

Site variety can be made quantitative by introducing information-theoretic indices.⁹ These are entropylike quantities computed by partitioning sites into equivalence classes by neighborhoods, which can be done in many different ways. For example, each site in Fig. 1(a) or 1(b) is either threefold coordinated with three adjacent rings of lengths l , m , and n , or it is twofold and adjacent to two rings of lengths l and m . Classes of a partition are thus denoted (l, m, n) or (l, m) . In ordered graphite, all sites are in $(6, 6, 6)$. Dividing the number of sites in each class by the total number of sites gives a probability which is used to define an entropy. Such an information-theoretic index thus quantifies site variety.⁹ Site variety in graphite, according to this partition, would be zero.

In the following we find exact recursion formulas for Green functions of several fractal-glass models. The effects of ring closure around the pore structure and of site variety on the one-electron spectral and transport properties are isolated and analyzed. In Sec. II, fractal glass models are introduced. Each of these models is related to the Sierpiński lattice treated by Domany, Alexander, Bensimon and Kadanoff.¹⁰ The methods for computing Green functions are reviewed in Sec. III.¹¹ Local densities of states (LDOS) and other spectral properties of the models are presented in Sec. IV. In Sec. V, eigenstates are discussed. The long-time average probability for propagation across the lattice is used to study electron localization as a function of lattice size and of energy E . Edge states are shown to be important in controlling transport from corner to corner. Effects of ring closure and site variety are investigated in Sec. VI. Ring closure is removed in two ways. In the first, branch cuts are introduced which replace the fractal by various Bethe-lattice approximations, or covering lattices. This also reduces site variety. Alternatively, rings are broken, resulting in fractal trees. Sec. VII is a summary.

II. MODELS

The graph in Fig. 1(b) is fourth in a hierarchy. The first graph in the sequence is a sixfold ring (benzene) and the second consists of three sixfold rings connected by three bonds (triphenylene). Graph $n + 1$ is defined by connecting three copies of graph n with three bonds, as in Fig. 2(a). In the limit of large n , the lattice becomes self-similar. This sequence defines model 1, or the triphenylene lattice. As a model for amorphous graphite it

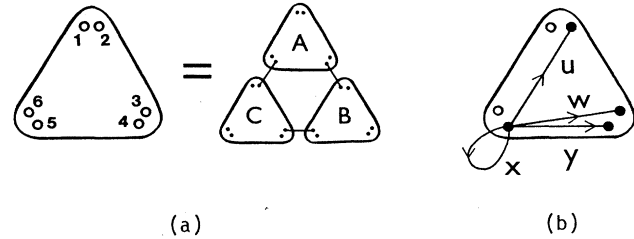


FIG. 2. Recursions for Fig. 1(b). (a) Generating relation; (b) Green functions x , y , u , and w .

is expected to be relatively stable because a large proportion of its rings are of length $4m + 2$ for some m .^{12,13}

The fourth graph in another hierarchy is shown in Fig. 3. The first graph is a single point (black dot) and the second consists of a sixfold ring with alternating black and white dots. Graph $n + 1$ is composed by connecting the corner sites (black) together with three bonds, each bond being decorated with a white vertex. Hence black sites become threefold coordinated while white dots retain twofold coordination. This sequence is model 2. In the large n limit, the lattice again becomes a fractal. As a model for amorphous graphite, the coloring may represent a difference between twofold and threefold sites. Extra valences would be saturated by hydrogens. Alternatively, the twofold and threefold sites may be occupied by different atoms, as in a two-dimensional (2D) Zachariasen glass.^{3,4,14}

The graphite interpretation of model 2 is not as plausible as that of model 1 because the $4m + 2$ rule is not as well satisfied, which leads to a large number of nonbonding states, as noted below.

The Zachariasen-glass interpretation becomes more interesting in a 3D version of the model. Thus, model 3 is a hierarchy generated by starting with a single black site and, at each iteration, connecting black corner sites of four copies of graph n together by six bonds, each decorated with a white site, to make graph $n + 1$. White sites are thus twofold and black sites fourfold coordinated. Model 3 is related to the diamond structure in the

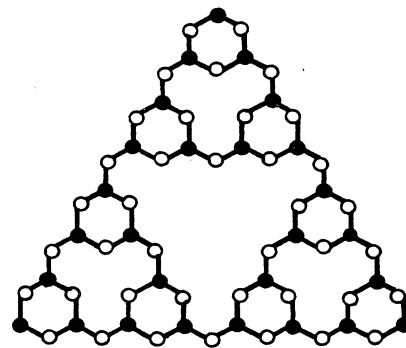


FIG. 3. 2D Zachariasen fractal glass.

same way model 2 is related to graphite. If black and white sites are considered chemically different, model 3 is a quartzlike Zachariasen glass.

Unfortunately, the fractal dimension of model 3 is only $\bar{d}=2$, so it is a rather unsubstantial model for a 3D glass. There are also many nonbonding and strongly localized states. Thus we next consider a more plausible 3D fractal-glass model.

The lattice of model 4 is a Cartesian product. The Cartesian product of two graphs A and B is defined as follows.^{15,16} Let $V(A)$ and $V(B)$ represent the vertex sets of A and B . If graph C is the Cartesian product of A and B , then its vertex set $V(C)$ is the Cartesian product of $V(A)$ with $V(B)$. $V(C)$ consists of all pairs (i, j) where $i \in V(A)$ and $j \in V(B)$. Adjacency on C must also be defined. Let vertices (i, j) and (k, l) be adjacent on C if either i is adjacent to k on A and $j = l$, or $i = k$ and j is adjacent to l on B . Hence, for example, the square lattice is a Cartesian product of two linear chains.

Graph n of model 4 is the Cartesian product of two copies of graph n of model 2. Ignoring the extreme corner points (of which there are only three) each site on model 2 is either twofold coordinated (white) or threefold coordinated (black). Thus sites on model 4 are fourfold (white), fivefold (gray), or sixfold coordinated (black).

The lattice of model 4 is a self-similar fractal with $\bar{d}=2 \ln 3 / \ln 2 \approx 3$ since graph $n+1$ is composed of nine copies of graph n . However, the number of bonds formed during the connection is not constant, as it is in models 2 and 3, but grows as 2^n . Thus model 4 is much more connected. While graph $n+1$ of model 2 or 3 can be separated into its graph- n components by severing only a small number of bonds, graph $n+1$ of model 4 cannot. The order of ramification of model 4 is not finite.^{6,7} Because of its higher ramification and its fractal dimension near 3, model 4 is a plausible fractal model for a Zachariasen glass of three components.

To each of the four models there corresponds a tight-binding one-electron Hamiltonian. The model Hamiltonian H corresponding to a given graph A is taken to be the adjacency matrix.^{17,18} The index set of H is $V(A)$, and $H_{i,j}=1$ if i and j are connected on A , otherwise $H_{i,j}=0$. The reason for choosing this austere approximation is simplicity. It has been mentioned that H plays two roles. As the adjacency matrix, it defines neighborhoods and hence the graph topology. As the Hamiltonian, it determines electronic behavior of the model via the discrete Schrödinger equation. For graphite models, one can think of H as the Hückel Hamiltonian of π -electron theory. In general, however, this simple form of H is chosen in order to isolate and simplify the relationship between adjacency of sites and properties of eigenstates. It is clear that the same mathematical model applies to the phenomena of lattice vibrations, spin waves, and diffusion by hopping, as well as to the linearized Ginzburg-Landau equation.¹⁹ The one-electron interpretation is used consistently in the current work.

III. GREEN FUNCTIONS

Spectral and transport properties are obtained from Green functions. The Green function $G_{ij}(z)$ is the i, j en-

try of the resolvent matrix

$$G(z) = (zI - H)^{-1} \quad (1)$$

defined for z outside the spectrum of H .

The method used to compute $G_{ij}(z)$ for a fractal hierarchy such as the sequence in model 1 is to express a small subset of Green functions for Hamiltonian $n+1$ in terms of the corresponding ones for Hamiltonian n . The resulting recursion relations thus give a particular set of Green functions on the entire sequence in terms of the solution for generation $n=0$. A symmetry-adapted version of this method was used by Alexander to treat a Sierpiński lattice in a magnetic field.¹⁹

The recursions for model 1 are constructed with reference to Fig. 2. A , B , and C are three copies of the graph for generation n . Linked together as shown they form generation $n+1$. Connecting sites on each of the subgraphs are numbered 1 through 6, so that site 1 on subgraph A is $A1$, and so on.

H_0 is the Hamiltonian for the three disconnected subgraphs. Thus H_0 is the direct sum of three copies of Hamiltonian n . Hamiltonian H for generation $n+1$ is given by

$$H = H_0 + V, \quad (2)$$

where the sparse matrix V has as its only nonzero entries the bonds connecting A , B , and C .

The necessary entries of

$$g(z) = (zI - H_0)^{-1} \quad (3)$$

for generation n are assumed known. Taking symmetry into account, the required elements of $g(z)$ are x , y , u , and w illustrated in Fig. 2(b). They are

$$\begin{aligned} x &= g_{11}(z), \\ y &= g_{61}(z), \\ u &= g_{41}(z), \\ w &= g_{51}(z). \end{aligned} \quad (4)$$

Inserting H from Eq. (2) into Eq. (1),

$$G(z) = g(z) + g(z)VG(z). \quad (5)$$

One next solves for the corresponding X , Y , U , and W of generation $n+1$:

$$\begin{aligned} X &= G(A1, A1) = x + wG(C2, A1) + uG(B1, A1), \\ Y &= G(C6, A1) = wG(A5, A1) + uG(B6, A1), \\ U &= G(B4, A1) = uG(A4, A1) + wG(C3, A1), \\ W &= G(C5, A1) = uG(A5, A1) + wG(B6, A1). \end{aligned} \quad (6)$$

The right-hand sides are evaluated by solving simultaneously

$$\begin{aligned}
G(C2, A1) &= xG(A5, A1) + yG(B6, A1), \\
G(B1, A1) &= xG(A4, A1) + yG(C3, A1), \\
G(A5, A1) &= w + xG(C2, A1) + yG(B1, A1), \\
G(B6, A1) &= xG(C3, A1) + yG(A4, A1), \\
G(A4, A1) &= u + xG(B1, A1) + yG(C2, A1), \\
G(C3, A1) &= xG(B6, A1) + yG(A5, A1).
\end{aligned} \tag{7}$$

The resulting recursion formulas are

$$\begin{aligned}
X &= x + [x(1+y^2-x^2-y)(u^2+w^2) \\
&\quad + 2y(y-y^2+x^2)uw]/\Delta, \\
Y &= [y(1-y)u^2 + 2xyuw + (1-y-x^2)w^2]/\Delta, \\
U &= [y(1-y)w^2 + 2xyuw + (1-y-x^2)u^2]/\Delta, \\
W &= [xy(u^2+w^2) + (1-x^2-y^2)uw]/\Delta,
\end{aligned} \tag{8}$$

where

$$\Delta = (1-x-y)(1+x-y)(1-x^2+y+y^2). \tag{9}$$

To obtain x, y, u, w for generation n in the family of model 1, one starts with Green functions for the sixfold ring:

$$\begin{aligned}
x &= z(z^2-3)u/2, \\
y &= (z^2-2)u/2, \\
u &= 2(z^2-1)^{-1}(z^2-4)^{-1}, \\
w &= zu/2,
\end{aligned} \tag{10}$$

and iterates Eqs. (8) and (9) $n-1$ times. Any other graph with sufficient symmetry could be used as a seed in place of a sixfold ring. Thus these recursions really represent a class of model hierarchies, modulo the initiating seed. When $w=u=y$, the recursions become the two-dimensional map $(x, y) \rightarrow (X, Y)$ for the Sierpiński lattice.¹¹

Model 2 is treated similarly. Referring to Fig. 3, let x be the diagonal Green function for one of the extreme corner sites black on generation n . Let y be from one such corner site to any other. To provide for the possibility that black and white sites are different, there is a diagonal site energy E_0 in the Hamiltonian for each white site. The Green function for a single isolated white site is $w = (z - E_0)^{-1}$. Proceeding as in the case of model 1 yields

$$\begin{aligned}
X &= x + 2wy^2(1-2wx)/\Delta, \\
Y &= wy^2[1-2w(x-y)]/\Delta,
\end{aligned} \tag{11}$$

where

$$\Delta[1-2w(x+y)][1-w(2x-y)]. \tag{12}$$

The value of w does not iterate, and w could in fact be scaled out of the equations: $r=wx, s=wy$.

Similarly, for model 3,

$$\begin{aligned}
X &= x + 3wy^2[1-2w(x-y)]/\Delta, \\
Y &= wy^2[1-2w(x-y)]/\Delta,
\end{aligned} \tag{13}$$

with

$$\Delta = (1-2wx)[1-2w(x+2y)]. \tag{14}$$

A single black site is used as a seed for either model 2 or model 3 so that $x=y=1/z$. Again, other seeds can be used, but strict triangle or tetrahedron symmetry is required.

Model 4 is not solved in the same way. Rather, because it is a Cartesian product of model 2 with itself, its Green functions are obtained as convolutions.¹¹

From the definition of model 4, the Hamiltonian K of its generation n is

$$K = H \otimes I + I \otimes H, \tag{15}$$

where H is Hamiltonian n of model 2, I is the identity on $V(H)$, and \otimes is the matrix direct product. If u_μ and u_ν are eigenvectors of H with eigenvalues E_μ and E_ν , then eigenvectors of k are each of the form^{15,16}

$$w_{\mu\nu} = u_\mu \otimes u_\nu, \tag{16}$$

with corresponding eigenvalue

$$E_{\mu\nu} = E_\mu + E_\nu. \tag{17}$$

The set $G(z)$ of Green functions for generation n of model 4 are found from the set $g(z)$ for model 2 by expanding in terms of eigenvectors and using Eqs. (15)–(17). The result is¹¹

$$\begin{aligned}
G_{(i,k)(j,l)}(z) \\
= -(1/\pi) \int_{-\infty}^{\infty} \text{Im}[g_{ij}(s+i\eta)]g_{kl}(z-s)ds.
\end{aligned} \tag{18}$$

Equation (18) defines any Green function on model 4 in terms of a pair on model 2.

The recursion relations obtained in this section give a certain subset of all Green functions for each model. Others are easily obtained by Eq. (5).

IV. LOCAL DENSITIES OF STATES

The local density of states (LDOS) at site i on the graph of H is²⁰

$$D_i(E) = \sum_{\nu} |u_{i\nu}|^2 \delta(E - E_\nu), \tag{19}$$

where $u_{i\nu}$ is component i of eigenvector u_ν with eigenvalue E_ν . For convenience,

$$\delta(E - E_\nu) = -(\eta/\pi) \text{Im}(E - E_\nu + i\eta)^{-1}, \tag{20}$$

so that each peak in Eq. (19) is broadened by a fixed amount η . The width η is adjusted to control the resolution.

From Eqs. (1), (19), and (20) one has the standard result²¹

$$D_i(E) = -(1/\pi) \text{Im}[G_{ii}(E + i\eta)]. \tag{21}$$

Thus the LDOS for connection sites (i.e., for the outermost corners on the generation n graph) of model 1, 2, or 3 is found from the imaginary part of X after $n-1$ iterations of Eqs. (8), (11), or (13). Model 4 is treated through the convolution in Eq. (18).

Figure 4 presents the LDOS for a corner site of model 1 at generation $n = 16$ (8.6×10^7 sites). The resolution η is a fixed ratio ($\frac{1}{250}$) of the energy range shown for each curve. Thus the relative resolution is constant. As the energy scale expands, successively higher levels of fine structure become visible. Peaks grow as the resolution becomes finer since the area under a given peak is fixed.

The entire spectrum is shown in Fig. 4(a). Symmetry about $E = 0$ is a consequence of the fact that the graph is bipartite,^{15,16} a property shared by all models treated here. The vertices of a bipartite graph can be painted with two colors so that each vertex is adjacent only to vertices of the opposite color. There is a pairing between an arbitrary eigenstate of energy E and another of energy $-E$. This consists of changing the signs of the eigenvector coefficients on sites of one of the two colors.²²

Since the off-diagonal Hamiltonian matrix entries are $+1$, the ground state, or state with eigenvector coefficients all of one sign, has a maximum eigenvalue E_{\max} . However, because of pairing one can think of $E_{\min} = -E_{\max}$ as the ground state. The reflection $E \rightarrow -E$ is equivalent to changing the off-diagonal H elements to -1 .

The perfect graphite lattice is also bipartite, and hence the LDOS is symmetric about $E = 0$. In contrast to model 1, the graphite LDOS is a smooth curve. Its Van

Hove singularities consist of steps at $E = \pm 3$, logarithmic peaks at $E = \pm 1$, and a parabolic zero at $E = 0$. Assuming two spin states and one electron per site, graphite is semimetal with its Fermi level at $E = 0$.

An essential difference between model 1 and graphite is that, as in the Sierpiński case,¹⁰ there is no continuum in the spectrum of model 1. That is, considered as a set of real numbers, the spectrum has no interior points. This property, which is typical of fractal lattices, is illustrated in Figs. 4(b)–4(e) showing successively higher resolution near $E = E_{\min}$. The small feature in the LDOS near $E = -2.5$ in Fig. 4(b) appears to be a relatively smooth curve. Figure 4(d) reveals its discontinuous fine structure. Successive magnification shows the structure repeating in a self-similar manner. The self-similarity is also typical of fractal lattices and is due to geometrical self-similarity of the eigenstates as E approaches E_{\max} of the nodeless ground state.

Near the ground state ($E \rightarrow E_{\max}$) the envelope of the total density of states (DOS) for a fractal behaves as $(E_{\max} - E)^c$, with $c = \frac{1}{2}\bar{d} - 1$, where the spectral dimension \bar{d} is the dimension of an effective wave-vector space.²³ For models 1 and 2, $\bar{d} = 2 \ln 3 / \ln 5 = 1.365$. The true density of states, like the LDOS, is highly singular and consists of a hierarchy of fine structure, but it scales as¹⁰

$$D(E_{\max} - \alpha \Delta E) \approx \alpha^c D(E_{\max} - \Delta E). \quad (22)$$

A 1D binary-alloy model with random substitutional disorder also shows hierarchical fine structure in its DOS at the band edge.²⁴ However, in the random-alloy case the DOS scales differently

$$\ln D(E_{\max} - \alpha \Delta E) \sim (E_{\max} - \alpha \Delta E)^{-p}, \quad (23)$$

with $p = \frac{1}{2}$. Band tails of this type occur quite universally in the case of random disorder due to geometrical correlation between fluctuations in the random potential.^{24,25} Thus the form of the band-edge DOS is a characteristic difference between ordered fractal-glass models and random models. However, there are band tails corresponding to localized states in both cases, and these cause hierarchical fine structure in the LDOS.

The peaks near $E = \pm 1.281$ (truncated) in Figs. 4(a) and (b) are localized triphenylene molecular states. They are symmetry decoupled from the rest of the lattice.

Figure 5(a) shows LDOS for a corner site (black) on model 2 ($n = 16$). $E_0 = 0$ is chosen since nonzero E_0 does not reduce symmetry and thus would remove no degeneracy. The spectrum is a noncontinuum with self-similarity near E_{\min} (or E_{\max}) as in model 1. Resolution is about $\frac{1}{120}$ of the range shown. The LDOS for this site is zero near $E = 0$, but the model contains a large number of localized nonbonding states with $E = 0$. These have amplitude only on the white sites and are localized on subgraph units of each length scale.

Due to a high degree of eigenstate localization, a typical LDOS on model 2 bears less resemblance to graphite than does a typical LDOS on model 1. The peaks in Fig. 5(a) are more tightly clustered. Eigenvalues are still more tightly grouped in model 3 due to an even higher degree

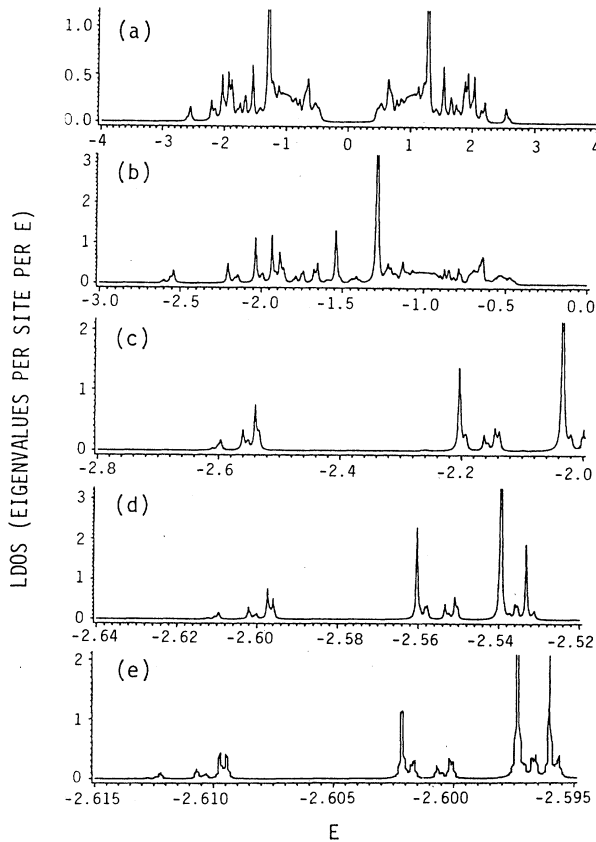


FIG. 4. LDOS for model 1. (a) Entire spectrum, (b) lower half, and (c)–(e) successively higher resolution near the ground state.

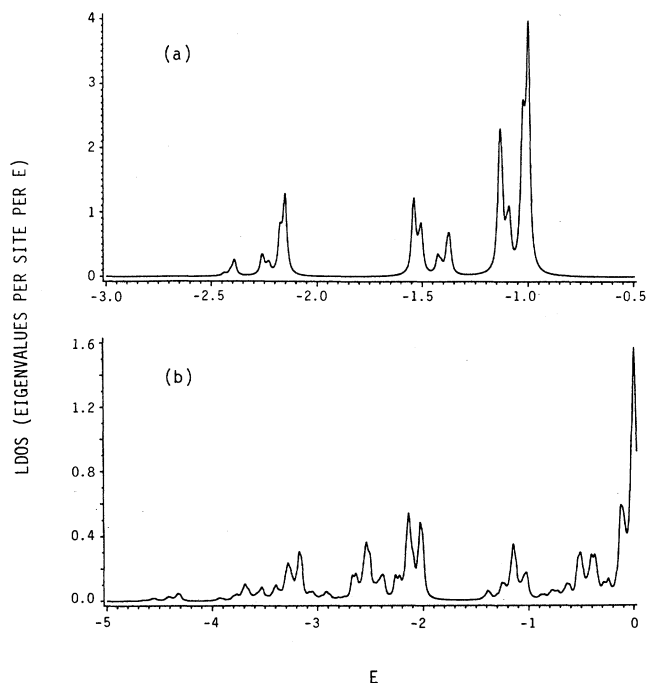


FIG. 5. LDOS at corner sites for (a) model 2 and (b) model 4.

of localization. To find a spectrum without as much empty space one must look at lattices with more connectedness. Hence, we proceed to model 4.

Figure 5(b) shows the LDOS for a corner site on model 4 obtained from iteration $n = 16$ of model 2 via Eq. (18). Self-similarity near $E = E_{\min}$ is inherited from model 2 through the convolution. Like the other fractal models, model 4 has no continuous part to its spectrum. However, the corner-point LDOS has more interesting structure, including states near zero.

For each of the models iterated, some of the eigenstates represented in the LDOS for the sites chosen are strongly localized while others are relatively extended. We turn to the topic of localization.

V. EIGENSTATES AND LOCALIZATION

A good example of a localized molecular state is provided by either of the two states on model 1 corresponding to the peaks in the LDOS on the corner site with $E \approx \pm 1.281$. As noted in the section above, they are due to a pair of states on the isolated triphenylene molecule, related by pairing, with $E = \pm[1 + (17)^{1/2}]/4$. These eigenstates have large amplitude on the corner site, but zero amplitude on the connecting sites where the triphenylene unit attaches to the rest of the fractal. Thus they do not couple into the glass, but remain localized molecular eigenstates of model 1 for each generation. There are other such molecular states.

Localized eigenstates of the fourfold-coordinated Sierpiński lattice are treated in the original paper by Domany *et al.* by means of decimation.¹⁰ Rammal also discusses the Sierpiński eigenstates.²⁶ Both papers include pictures of amplitude patterns of certain states.

The eigenstates of models 1, 2, and 3 presented here have general properties in common with those of the Sierpiński case,²⁶ which is reviewed here briefly.

At a given generation n , each eigenstate on the Sierpiński lattice is either new or is related by decimation to a state of the previous generation $n - 1$. Eigenvalues of the new states are $E = -1$ or $E = -2$. Eigenvectors can be chosen so that $E = -1$ states are internal surface states bounding the voids. New states with $E = -2$ are edge states, as illustrated in Fig. 6(a). States not new at generation n are of one of three types: (i) the ground state $E = +4$, (ii) descended from the $E = +2$ state on generation $n = 1$ (triangle), or (iii) descended from $E = -1$ or $E = -2$ on generation $n - 1$. Thus, at each generation, there are states localized at various length scales associated with the voids of the pore structure, and there are edge states and other, related states.

The nonbonding states of model 2 have zero amplitude on black sites and alternate ± 1 on white sites forming closed, self-avoiding walks of length $4m$. An orthogonal set can be chosen around boundaries of each void with perimeter 12 or larger. The nonbonding states are in this way associated with the pore structure in model 2.

There are also surface states bounding the external edges of model 2 as a whole and of each of its subgraphs. These are superpositions of benzene molecular states with $E = \pm 1$. Consider one of the outer edges. Let the amplitude on each white site on the edge be zero. To form the edge state with $E = +1$, choose one black edge site and assign it amplitude $+1$. The white site backbonded to it would also have amplitude $+1$, while second-neighbor black sites on the edge would have -1 , and their backbonded white sites $+1$, and so on. Corners are not difficult to make, and thus states can be constructed that are localized on any length scale. Such states contribute to the peaks at $E = \pm 1$ in the LDOS for the corner site of model 2 as shown Fig. 5(a).

Eigenstates of model 4 are direct products of pairs of eigenstates of model 2. Thus there are nonbonding states associated with the inner surfaces of the toroidal voids that make up the pore structure of model 4. There are also surface states bounding model 4 as a whole and bounding each subgraph. These contribute to the peaks at $E = \pm 2$ and at $E = 0$ in the corner-point LDOS of Fig. 5(b).

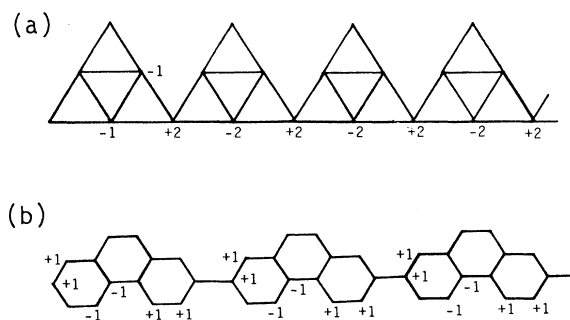


FIG. 6. Edge states. (a) Fourfold Sierpiński lattice with $E = -2$; (b) model 1 with $E = +1$.

Edge states on model 1 play an interesting role in determining electron transport properties. An amplitude pattern for one of these is shown in Fig. 6(b) where it is compared with an edge state of the Sierpiński lattice in Fig. 6(a). An edge state of this kind would connect sites on opposite corners. On model 1 the edge-state energies are $E = \pm 1$.

As a measure of electron transport we use the corner-to-corner propagation amplitude.^{27,28} Let $|j(t)\rangle$ be the state evolved from basis state $|j\rangle$ at $t=0$. The probability of finding an electron at site i at time t , given an electron at site j at $t=0$ is $|\langle i|j(t)\rangle|^2$. Integrating over time gives

$$P_{ij} = \int_0^\infty |\langle i|j(t)\rangle|^2 dt = (2\pi)^{-1} \int_{-\infty}^\infty |G_{ij}(E)|^2 dE . \tag{24}$$

The integrals converge for finite η . P_{ij} is a measure of the long-time likelihood for propagation from j to i . Selecting corner points $j=2, i=5$ from Fig. 2, define

$$P_n = (2\pi)^{-1} \int_{-\infty}^\infty |u_n(E + i\eta)|^2 dE , \tag{25}$$

where u_n is obtained by n iterations of Eqs. (7) and (8).²⁹

Unlike conductivity or other bulk transport properties, P_n depends in detail on the way the eigenstates couple to the pair of chosen sites. Nevertheless, P_n provides a convenient way to look at transport across the lattice as a function of lattice size. Figure 7 shows P_n versus generation number n . The length of an edge is $L \sim 2^n$.

Power-law behavior is seen in Fig. 7(a), which shows a best-fit line through computed values of $\ln(P_n/P_0)$ versus n for $n < 6$. The slope $-1.11 (\approx -\ln 3)$ is consistent with $P_n \sim L^{-\bar{d}}$, where \bar{d} is the fractal dimension. This would

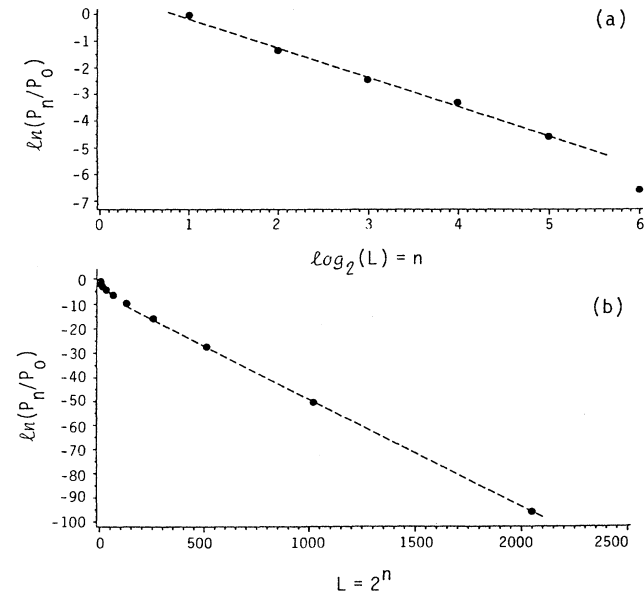


FIG. 7. Scaling of propagation probability for model 1. (a) L below the correlation length; (b) L exceeding the correlation length.

be expected if the wave function were spreading out uniformly over available sites out to a correlation length $\lambda \sim 2^6 = 64$.

Beyond $L = \lambda$, exponential decay sets in. Figure 7(b) shows that $\ln(P/P_0)$ becomes linear in L , or, in other words, P_n is proportional to $e^{-\nu L}$. Here $\nu = 0.045$.

The transition to exponential behavior beyond $L = \lambda$ is similar to the behavior of conductance of the Anderson model for homogeneous disorder, to which well-known scaling arguments apply.³⁰ P_n is a different measure of eigenstate localization and the current models are not homogeneous or random. However, localization in either case is manifested in the existence of a growing proportion of molecular or standing-wave states as lattice size increases. Scaling arguments for conductance in the fractal case have been suggested by Rammal and Toulouse.³¹

It is interesting to resolve P_n into contributions from eigenstates at various energies. Figure 8 shows corner-to-corner propagation per E as given by $|u_n(E + i\eta)|^2$ for generations $n=3, 6$, and 8 of model 1. For $n=3, L < \lambda$, and propagation occurs at many energies. Thus the curve in Fig. 8(a) resembles the LDOS of Fig. 4(a). For $n=8, L > \lambda$, and propagation is in narrow energy channels near $E = \pm 1$, as seen in Fig. 8(c). The intermediate case $n=6$ with $L \approx \lambda$ is shown in Fig. 8(b).

The propagation from corner to corner for large L takes place mainly via the edge states as shown in Fig.

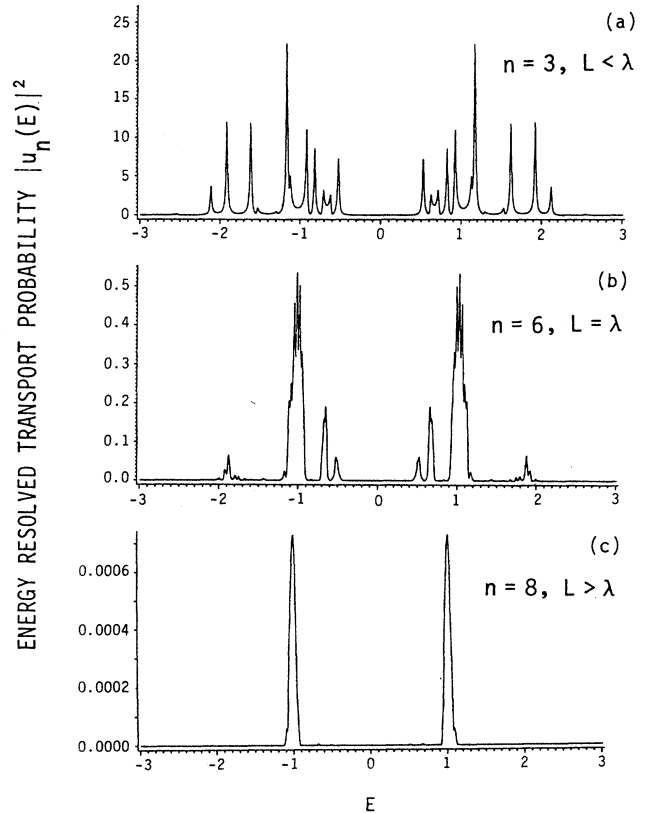


FIG. 8. Channeling of propagation as a function of E . (a) L below, (b) L near, and (c) L exceeding the correlation length.

6(b) and via states that evolve from edge states as the subgraphs of generation n are joined together forming generation $n + 1$ of the lattice. The energies of these are near ± 1 and the amplitude patterns zigzag along the subgraph edges. Edge states in the case of homogeneous random disorder play a role in the quantum Hall effect.^{32,22}

VI. RING CLOSURE AND SITE VARIETY

Eigenstate localization is a common property of the hierarchical models. In the random networks, where localization also occurs for sufficient disorder, it is associated with noncontinuum regions of the spectrum.³⁰ As a function of structural parameters the spectra of either the random or the hierarchical models may or may not contain continua. Because of the similarities between these two kinds of models, the existence of hierarchical lattice Hamiltonians with spectral continua but all eigenstates localized suggests two questions.¹¹ The first is whether there is a continuum-delocalization region in the homogeneous random but not in the hierarchical case. The second is whether geometrical properties such as site variety, ring structure, or (especially in the fractal case) connectedness can be correlated with spectral properties. It is this latter question that will be pursued here.

It is possible to remove the effects of ring closure and site variety in varying degrees by introducing branch cuts. These unwind rings by making the lattice multisheeted. To do this, the recursive definition of model 1 is modified so that after a certain generation k the lattice becomes an infinitely branching Bethe tree.³⁴

As an example, consider a benzene ring. A walk around the ring encounters the original site after six steps. If a cut is introduced, then after six steps the walk encounters not the original site but another identical copy of it. The ring is thus transformed into the infinite chain, which is its universal covering graph.³⁵ The original ring is recovered by identifying every sixth site on the chain as the same site. The Green functions for the ring can be found as a sum over the chain Green functions connecting sites that are equivalent modulo the sixfold ring. Thus one can keep track of contributions to the ring Green functions due to paths winding around the ring a certain number of times.

The similar introduction of a cut in each ring of a square lattice yields as its universal covering a fourfold-coordinated Bethe lattice.³⁶

The strategy here is to begin by cutting each ring in the fractal graphite model 1, except for the elementary sixfold rings of the seed, thus forming a Bethe-lattice covering. Then, by systematically reconnecting rings of increasing length, the effects of ring closure on the spectrum are studied.

Figure 9 shows in symbolic form the method of generating Bethe-lattice coverings of model 1. After iterating the recursive definition of model 1 $k - 1$ times, the resulting graph is used as a seed initiating the sequence of Fig. 9. The result after many iterations is a Bethe lattice, each unit cell of which is graph k of model 1. Thus it is a multisheeted model in which all rings of model 1 up to generation k are included normally but all larger rings

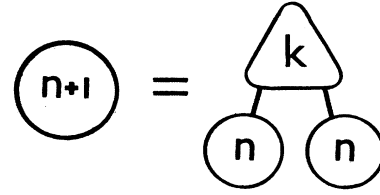


FIG. 9. Recursive definition of Bethe covering lattice. The k th generation of model 1 is used as a seed to grow a Bethe lattice.

have been unwound by the introduction of branch cuts.

From Fig. 9, one finds that the Green function g for the corner site at the top of a multisheeted covering satisfies

$$g = x + g [(u^2 + w^2)(1 - xg) + 2uwyg] / \Delta, \quad (26)$$

where

$$\Delta = [1 - g(x + y)][1 - g(x - y)], \quad (27)$$

and x , y , u , and w are obtained from the $(k - 1)$ th iteration of Eqs. (8) and (9). Unlike the fractal case, Eqs. (26) and (27) iterate to a fixed point. The physical Green function is the root of

$$(x^2 - y^2)g^3 + [x(u^2 + w^2) - 2(uwy + x)]g^2 + (1 - u^2 - w^2)g - x = 0, \quad (28)$$

which approaches x as u , v , w , and y tend to zero. This root is most easily obtained by iterating Eqs. (26) and (27).³⁶

Figure 10 shows the effect on the LDOS of closing rings of various lengths. Only the sixfold rings of the seed are closed in Fig. 10(a), corresponding to $k = 1$. In Fig. 10(b), for which $k = 2$, all rings in the triphenylene units are closed, so the model consists of a Bethe lattice with triphenylene unit cells. In the case $k = 3$, for which all rings on the next generation are closed, the LDOS is almost indistinguishable from the limit $k \rightarrow \infty$ shown in Fig. 10(c) for this choice of resolution. However, the spectrum is actually composed of finite, continuous bands for any finite value of k . This is because u , w , y , and x are rational functions, so g can be seen from Eq. (28) to be algebraic of finite degree in E .

It is well known that the low-order moments of the LDOS must be reproduced accurately by the cluster-Bethe-lattice scheme employed here.²¹ The first discrepant moment with respect to E of the LDOS (Refs. 37 and 38) is determined by the length of the shortest closed walk present on model 1, but absent in the covering k . However, it is interesting that the Bethe lattice reproduces the detailed shape of the LDOS for rather low k , even for such a pathological spectrum.

The Bethe-lattice coverings remove closed rings, and at the same time they permit continua to condense in the spectrum. The continuous energy bands dissociate into a fractal as successively longer closed rings are reintroduced. However, it is *wrong* to conclude that ring closure causes the dissociation, since as the Bethe lattice removes

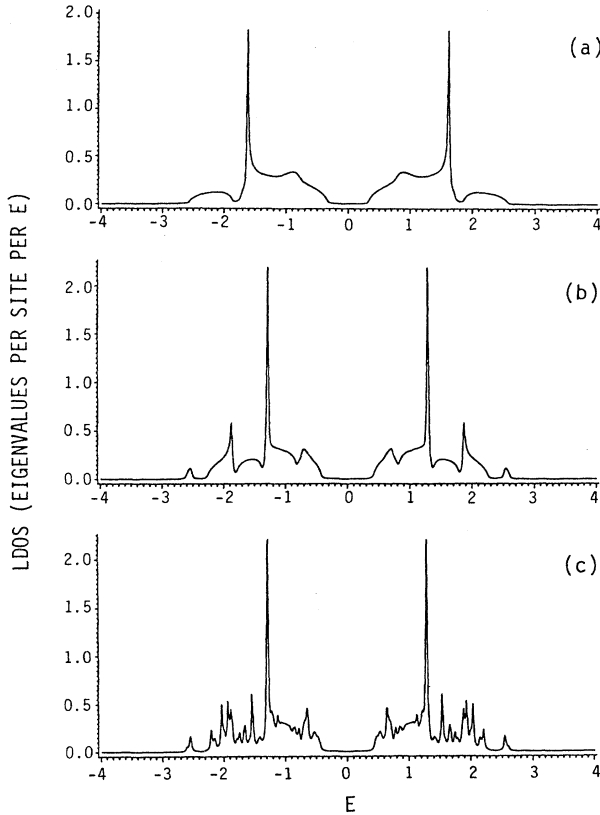


FIG. 10. LDOS for various coverings. (a) Only the benzene rings, (b) all triphenylene rings, and (c) all rings are closed.

rings it *also reduces site variety*. At a point far from the root of the $k = 1$ Bethe lattice, there are only six distinct site environments, since the unit cell consists of a sixfold ring. Thus, removing rings by introducing cuts does not discriminate between the effects of ring closure and site variety.

To remove rings without eliminating variation in site environments, we modify model 1 in a different way. If after generation k the bond between subgraphs B and C in Fig. 2(a) is cleaved for all successive generations, the result is a new kind of fractal tree. All rings are as in model 1, up to generation k , but all larger rings are disconnected, i.e., broken. Since the model is still a fractal there is still fluctuation in the site environments, but rings are removed.

Breaking the link between subgraphs b and C in Fig. 2(a) reduces the symmetry. Thus another distinct Green function must enter the recursion. The diagonal Green function x at the root site is now distinct from the one at a lower connection site, which we shall call v . Following the procedure of Sec. III, one has

$$\begin{aligned}
 X &= x + x[(u^2 + w^2)(1 - xv) + 2uwx] / \Delta, \\
 Y &= u^2 y / \Delta, \\
 U &= u[u(1 - xv) + wxy] / \Delta, \\
 V &= u[v(1 - xv) + xy^2] / \Delta, \\
 W &= u[w(1 - xv) + uxy] / \Delta,
 \end{aligned} \tag{29}$$

where

$$\Delta = [1 - x(v + y)][1 - x(v - y)]. \tag{30}$$

To treat the lattice formed from generation k of model 1, one starts with x , y , w , and u given in Eqs. (10) for the benzene seed and iterates Eqs. (29) and (30) $k - 1$ times. The resulting values of x , y , w , u and $v = x$ are then used to seed Eqs. (23) and (24) which are iterated as many times as necessary.

The root-site LDOS of the trees constructed in this way do not show continuous ranges of eigenvalues. Whatever the value of k chosen, the spectrum of the tree model, like that of each of the other fractal models, does not contain any interior points.

The difference between the generation k of the Bethe lattice and of the tree lattice is not in connectedness or in ring closure. Both are quasi-1D in the sense that major portions of the graph of either model can be separated by cleaving only one bond. The essential difference is in the variety of site environments. For $k = 1$, there are only six different kinds of sites deep in the Bethe lattice, while the sites of the fractal tree maintain variety by being connected by different numbers of steps to branches of different sizes.

Joannopoulos has studied the relative importance of ring closure and site variety in determining features of the LDOS in homogeneous models of amorphous semiconductors using a Bethe-lattice approximation.³⁹ Bond-angle fluctuations rather than ring closure were found to determine the shape of the LDOS near the top of the valence band in these homogeneous models.

VII. SUMMARY

The models studied above are simple tight-binding one-electron Hamiltonians on hierarchical lattices. An important characteristic which they share with homogeneous random networks is that the detailed environments of the individual sites fluctuate considerably. Because of the scaling properties of their pore structures they are also trema fractals.

The local bonding of model 1 shown in Fig. 1(b) is like porous graphite. Figure 2 shows model 2, which is a 2D Zachariasen glass of two components. Model 3 is the 3D analog of model 2, thus representing a quartzlike fractal glass. Unfortunately, since the fractal dimension of model 3 is only $\bar{d} = 2$, it is not a good model of a 3D glass. Thus, model 4 is constructed as the Cartesian product of model 2 with itself. Model 4 has fractal dimension $\bar{d} \approx 3$ and spectral dimension²³ $\bar{d} \approx 2.7$, and it is infinitely ramified.⁷ Each model comprises a hierarchy of Hamiltonians $\{H_n\}$, the generation $n + 1$ Hamiltonian H_{n+1} being defined in terms of H_n .

The principal analytical results of the work reported here are the recursion formulas of Sec. III which express exactly Green functions for generation $n + 1$ in terms of those for generation n for models 1, 2, and 3. Green functions for model 4 are given as convolutions in Eq. (18). Each set of recursion formulas could also be used to study other hierarchical families by varying the seed H_0 , and extension theory could be used to include the effects

the effects of second-neighbor interactions.¹¹

Certain eigenstates can be identified as localized molecular states that have become symmetry decoupled from the bulk of the glass. There are states associated with the inner surfaces bounding the voids of the pore structure, and other states associated with outer surfaces or edges bounding the lattice as a whole as well as each subunit. Thus, eigenstates are localized in a hierarchical way on every length scale.

The time-integrated corner-to-corner propagation probability P_n for generation n is used to study localization on model 1 in Sec. V. Figure 7 shows that $P_n \sim L^{-d}$ until the lattice size $L \approx \lambda = 64$, then at larger L , $P_n \sim e^{-\nu L}$. This transition from power-law to exponential behavior is similar to that of electrical conductance in the case of random disorder.²⁹⁻³¹ In model 2, there is no power-law behavior ($\lambda \approx 0$) and the exponential drop begins right away. Edge states with $E = \pm 1$ as shown in Fig. 5(b) participate to an increasing extent in the corner-to-corner propagation on model 1 as $L \rightarrow \infty$.

The effects of ring closure and site variety are explored in Sec. VI, where two new models are introduced.

In the first modification, model 1 is iterated normally up to generation k , beyond which branch cuts are inserted in the recursive definition. The result is a Bethe lattice with generation k of model 1 as a unit cell. Green functions for this modification are given by Eqs. (26) and (27). The resulting spectrum is a collection of continua over small energy ranges. However, the Bethe-lattice LDOS forms a smooth envelope that fits the main features of the corresponding LDOS for model 1 very well for small k .

In the second modification, model 1 is again iterated normally up to generation k , beyond which all rings of a longer scale are broken by severing the connecting bonds. This results in a fractal tree on which each unit cell is

generation k of model 1. Green functions are given by Eqs. (29) and (30). Here the resulting spectrum has the noncontinuum structure of a typical fractal.

The difference between the two modifications is not in connectedness¹⁹ or in ring closure¹³ but in site variety.³⁰ It is suggested that localization of eigenstates and the lack of continua in the spectrum in these fractal-glass models may best be understood in terms of the Anderson mechanism.³⁰ In both the random networks and the hierarchical fractals, localized states result from the superposition of reflected waves with incommensurate phases caused by the fluctuation in site environments.

One could easily include two additional effects that have not been treated here. The existence of rings of odd length is known to be important in determining properties of glasses.⁵ Odd rings could be introduced by modifying the models slightly. The Sierpiński lattice contains odd rings. Also, a true random potential could be added to the fractal models by drawing subunit components from a statistical distribution at each stage in the iterative definition. Rigorous self-similarity in the LDOS of ordered fractal models is a consequence of self-similarity in the geometry. The exact nature and energy of the edge states also depends on the detailed regularity. Were one to include randomness in the hierarchical definition of the lattice, the self-similar fine structure would be destroyed, but the fractal scaling law Eq. (22) would remain valid in a random fractal-glass model.²³ This is quite different from the Urbach form of the band tails in homogeneous random networks.²⁵ Edge states would also be expected in the random fractal case as in the homogeneous random case. Thus no essentially new features are expected to appear if randomness were added to the definition of the ordered fractal-glass models treated in this work.

¹F. Yonezawa and T. Ninomiya, in *Topological Disorder in Condensed Matter*, Vol. 46 of *Springer Series in Solid-State Sciences*, edited by F. Yonezawa and T. Ninomiya (Springer-Verlag, Berlin, 1983).

²J. Ziman, *Models of Disorder: The Theoretical Physics of Homogeneously Disordered Systems* (Cambridge University Press, Cambridge, England, 1979).

³R. Zallen, *J. Non-Cryst. Solids* **75**, 3 (1985).

⁴M. Klinger, *Phys. Rep.* **165**, 277 (1988).

⁵N. Rivier, in Ref. 1.

⁶B. Mandelbrot, *Fractal Geometry of Nature* (Freeman, San Francisco, 1982).

⁷Y. Gefen, A. Aharony, B. Mandelbrot, and S. Kirkpatrick, *Phys. Rev. Lett.* **21**, 1771 (1981).

⁸H. Bale and P. Schmidt, *Phys. Rev. Lett.* **53**, 596 (1984).

⁹D. Bonchev and N. Trinajstić, *J. Chem. Phys.* **67**, 4517 (1977); S. Basak, V. Magnuson, G. Niemi, R. Regal, and G. Veith, *Math. Modeling* **8**, 300 (1987).

¹⁰E. Domany, S. Alexander, D. Bensimon, and L. Kadanoff, *Phys. Rev. B* **28**, 3110 (1983).

¹¹W. Schwalm and M. Schwalm, *Phys. Rev. B* **37**, 9524 (1988).

¹²M. Dewar, *The Molecular Orbital Theory of Organic Chemistry* (McGraw-Hill, New York, 1969), p. 177.

¹³I. Gutman and N. Trinajstić, *Chem. Phys. Lett.* **20**, 257 (1973).

¹⁴W. Zachariasen, *J. Am. Chem. Soc.* **54**, 3841 (1932).

¹⁵D. Cvetković, M. Doob, and H. Sachs, *Spectra of Graphs and Applications* (Academic, New York, 1980), pp. 65-72 and references therein.

¹⁶A. Shwenk and R. Wilson, in *Selected Topics in Graph Theory*, edited by L. Beineke and R. Wilson (Academic, London, 1978).

¹⁷E. Hückel, *Z. Phys.* **70**, 204 (1931).

¹⁸R. McWeeny, *Coulson's Valence*, 3rd ed. (Oxford University Press, London, 1979).

¹⁹S. Alexander, *Phys. Rev. B* **29**, 5504 (1984).

²⁰J. Friedel, *Adv. Phys.* **3**, 446 (1954).

²¹R. Haydock, V. Heine, and M. Kelly, *J. Phys. C* **5**, 2845 (1972).

²²C. Coulson, *Proc. Cambridge Philos. Soc.* **46**, 202 (1940).

²³S. Alexander and R. Orbach, *J. Phys. (Paris) Lett.* **43**, L625 (1982).

²⁴J. Gubernatis and P. Taylor, *J. Phys. C* **6**, 1889 (1973).

- ²⁵V. Sa-Yakanit and H. Glyde, *Comments Condensed Matter Phys. B* **13**, 35 (1987).
- ²⁶R. Rammal, *J. Phys. (Paris)* **45**, 191 (1984).
- ²⁷L. Roof and J. Skinner, *Phys. Rev. B* **33**, 7738 (1986).
- ²⁸T. Odaski and K. Chang, *Phys. Rev. B* **30**, 1612 (1984).
- ²⁹E. Abrahams, P. Anderson, D. Liccardello, and D. Ramakrishnan, *Phys. Rev. Lett.* **42**, 673 (1979).
- ³⁰P. Anderson, *Phys. Rev.* **109**, 1492 (1958).
- ³¹R. Rammal and G. Toulouse, *J. Phys. (Paris) Lett.* **44**, L13 (1983).
- ³²B. Halperin, *Phys. Rev. B* **25**, 2185 (1982).
- ³³A. MacKinnon, L. Schweitzer, and B. Kramer, *Surf. Sci.* **142**, 189 (1984).
- ³⁴H. Bethe, *Proc. R. Soc. London, Ser. A* **216**, 45 (1935).
- ³⁵J. Stillwell, *Classical Topology and Combinational Group Theory* (Springer, New York, 1980), Chap. 2.
- ³⁶R. Laughlin and J. Joannopoulos, *Phys. Rev. B* **16**, 2942 (1977).
- ³⁷F. Cyrot-Lackmann, *J. Phys. Chem. Solids* **29**, 1235 (1968).
- ³⁸J. Burdett, S. Lee, and W. Sha, *Croatica Chem. Acta* **57**, 1193 (1984).
- ³⁹J. Joannopoulos, *Phys. Rev. B* **16**, 2764 (1977).